PAPER

Check for updates

Stability analysis for heat transfer flow in micropolar hybrid nanofluids

Nur Hazirah Adilla Norzawary,[a] Siti Khuzaimah Soid,[b] Anuar Ishak, [c]
Muhammad Khairul Anuar Mohamed,[d] Umair Khan, *[cef] El-Sayed M. Sherif [g]
and Ioan Pop[h]

Objective: hybrid nanofluids have superior thermal efficiency and physical durability in contrast to regular nanofluids. The stagnation point flow of MHD micropolar hybrid nanofluids over a deformable sheet with viscous dissipation is investigated. *Methodology*: the controlling partial differential equations are converted to nonlinear ordinary differential equations using the transmuted similarity, and are subsequently solved using the bvp4c solver in MATLAB. The hybrid nanofluids consist of aluminum and copper nanoparticles, dispersed in a base fluid of water. *Results*: multiple solutions are obtained in the given problem for the case of shrinking as well as for the stretching sheet due to the variation in several influential parameters. Non-unique solutions, generally, exist for the case of shrinking sheets. In addition, the first branch solution is physically stable and acceptable according to the stability analysis. The friction factor is higher for the branch of the first solution and lower in the second branch due to the higher magnetic parameters, while the opposite behavior is seen in the case of the local heat transfer rate. *Originality*: the novelty of this model is that it finds multiple solutions in the presence of Cu and Al_2O_3 nanoparticles and also performs the stability analysis. In general, non-unique solutions exist for the phenomenon of shrinking sheets.

aInstitute for Mathematical Research, Universiti Putra Malaysia, 43400 Serdang, Selangor, Malaysia. E-mail: nurhazirah.adilla@gmail.com

bSchool of Mathematical Sciences, College of Computing, Informatics and Media, Universiti Teknologi MARA, 40450 Shah Alam, Selangor, Malaysia. E-mail: khuzaimah@tmsk.uitm.edu.my

cDepartment of Mathematical Sciences, Faculty of Science and Technology, Universiti Kebangsaan Malaysia, UKM Bangi, 43600, Selangor, Malaysia. E-mail: anuar_mi@ukm.edu.my; umair.khan@lau.edu.lb

dCentre for Mathematical Sciences, College of Computing and Applied Sciences, Universiti Malaysia Pahang, Gambang, 26300, Pahang, Malaysia. E-mail: m.k.a.mohamed@gmail.com

eDepartment of Computer Science and Mathematics, Lebanese American University, Byblos, Lebanon

fDepartment of Mathematics and Social Sciences, Sukkur IBA University, Sukkur 65200, Sindh, Pakistan

gCenter of Excellence for Research in Engineering Materials (CEREM), Deanship of Scientific Research, King Saud University, Riyadh 11421, Saudi Arabia. E-mail: esherif@ksu.edu.sa

hDepartment of Mathematics, Babeş-Bolyai University, 400084 Cluj-Napoca, Romania. E-mail: Popm.ioan@yahoo.co.uk

1. Introduction

Stagnation point flow represents the attributes of fluid flow as it meets and interacts with a solid surface. At the location where the fluid comes to a halt upon meeting the surface, it separates into several streams, giving rise to the stagnation point flow effect. Hiemenz[1] is the pioneer who explored the stagnation point flow due to a semi-infinite static wall. In addition, research on micropolar fluid flow has captivated many scientists because of its numerous applications including the extrusion of polymer fluids and liquid crystal solidification. The micropolar fluid theory was initiated by Eringen.[2] The micro-rotational effect and the micro-rotational inertia are demonstrated by these fluids. Eventually, many researchers implement Eringen's idea in various problems such as Soid *et al.*[3] who studied micropolar fluid magnetohydrodynamics (MHD) stagnation point flow with slip. Next, a micropolar fluid with a mixed convection flow was scrutinized by Khashi'ie *et al.*[4] Furthermore, there are more studies on micropolar fluids.[5–7]

The demand for nanofluids in industrial applications has led to extensive research on their properties. One of the primary reasons for this interest is their ability to significantly enhance heat transfer in various fields, including electronics, transportation, and biomedicine. The nanofluid concept was first proposed by Choi.[8] Since then, nanofluids have found extensive use in solar thermal applications, industrial cooling applications, and many other fields. Numerous researchers have examined the nanofluid, including Rahman *et al.*,[9] Norzawary *et al.*[10] and Wahid *et al.*[11] Less research has been done on micropolar nanofluids, though. Hussain *et al.*[12] examined the micropolar nanofluid *via* stretching sheets numerically. Following them, Patel *et al.*,[13] Lund *et al.*,[14] Atif *et al.*[15] and numerous others have investigated various surfaces and angles of the micropolar nanofluid flow problem.

The term "hybrid nanofluid" involves a new sort of nanofluid that contains a base fluid mixed with two types of nanoparticles, leading to an effective enhancement in heat transfer. Extensive research has shown a significant improvement in the heat conductivity of this novel fluid, as seen in studies by Madhesh and Kalaiselvam[16] and Devi and Devi.[17] Therefore, many researchers have focused on investigating the mathematical aspects of the boundary layer flow in hybrid nanofluids, particularly on stretching/shrinking sheets.[18–24] For instance, Subhani and Nadeem[25] explored the micropolar flow for hybrid (Cu/TiO$_2$/water) nanofluids and claimed that the heat flow capability of a micropolar hybrid nanofluid is much better in comparison to that of a micropolar nanofluid. It appears that there has been little research on micropolar hybrid nanofluids. Hence, the primary aim of this work is to examine how stretching and contraction of the surface affect the behaviour of a micropolar hybrid nanofluid.

The magnetohydrodynamic (MHD) effect is also important. MHD has great impacts on engineering due to its vital principles. These principles are also applied in numerous industrial applications such as MHD pumps, generators, nuclear reactor cooling, flow meters, heat exchangers, nuclear waste disposal, geothermal energy extractors, and space vehicle impulsion. The presence of a magnetic effect produces a Lorentz force generated by the magnetic field which usually repels the hydrodynamic field in the presence or absence of a permeable matrix. The MHD flow of micropolar nanofluid *via* a stretch surface was researched by Kamal *et al.*[26] and Yasmin *et al.*[27] However viscous dissipation is the process in which shear forces influence a fluid on the adjacent layers and transform into heat, and represented by the Eckert number, which is also considered in this work. Some authors who considered this effect are Hsiao[28] and Lund *et al.*[29] both of whom studied the micropolar nanofluid flow *via* stretching sheets.

As a result of the abovementioned research, we are driven to explore the MHD and viscous dissipation effects and to expand Anuar *et al.*[30] work by implementing the stagnation point. We aim to provide a mathematical model for the problem and observe the impact of the considered parameters on the physical quantities of interest to simulate the fluid flow dynamics *via* the numerical perspective. These numerical findings (simulation of the fluid behaviour) could serve as guidance to those working with the fluid in experimental and practical activities. In addition, this analysis also comprises a novel era for scientists to discover the shrinking features of micropolar hybrid nanofluids. Furthermore, the novelty of this study can also be seen in the discovery of non-unique solutions and the execution of stability analysis.

2. Mathematical modeling of the problem

2.1. The description of governing equations with boundary conditions (BCs)

Consider a 2D steady incompressible stagnation point flow of magnetohydrodynamic (MHD) micropolar Cu–Al$_2$O$_3$/H$_2$O nanofluid past a deformable sheet as pictured in Fig. 1. Both the velocity of stretching/shrinking and that of a fluid in the far-
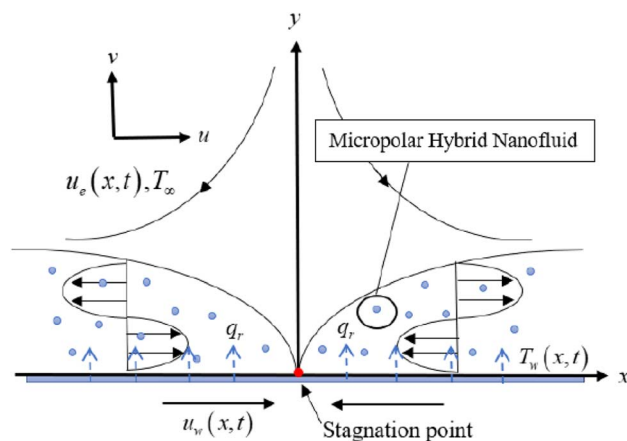

Fig. 1 Physical model of shrinking flow (Anuar *et al.*[28]).

field, denoted as $U_w(x) = ax$ and $U_\infty(x) = bx$, exhibit a linear variation from the stagnation point which a and $b(>0)$ are constants. The model is formulated as (Soid *et al.*[3] and Anuar *et al.*[30]):

$$\frac{\partial u}{\partial x} + \frac{\partial v}{\partial y} = 0, \tag{1}$$

$$u\frac{\partial u}{\partial x} + v\frac{\partial u}{\partial y} = U_\infty \frac{\mathrm{d}U_\infty}{\mathrm{d}x} + \left(\frac{\mu_{\mathrm{hnf}} + \kappa}{\rho_{\mathrm{hnf}}}\right)\frac{\partial^2 u}{\partial y^2} + \frac{\kappa}{\rho_{\mathrm{hnf}}}\frac{\partial N}{\partial y}$$
$$+ \frac{\sigma_{\mathrm{hnf}} B_0^2}{\rho_{\mathrm{hnf}}}(U_\infty - u), \tag{2}$$

$$u\frac{\partial N}{\partial x} + v\frac{\partial N}{\partial y} = \frac{\varsigma}{\rho_{\mathrm{hnf}}j}\frac{\partial^2 N}{\partial y^2} - \frac{\kappa}{\rho_{\mathrm{hnf}}j}\left(2N + \frac{\partial u}{\partial y}\right), \tag{3}$$

$$u\frac{\partial T}{\partial x} + v\frac{\partial T}{\partial y} = \frac{k_{\mathrm{hnf}}}{(\rho C_p)_{\mathrm{hnf}}}\frac{\partial^2 T}{\partial r^2} + \frac{\sigma_{\mathrm{hnf}} B_0^2}{(\rho C_p)_{\mathrm{hnf}}}(U_\infty - u)^2$$
$$+ \frac{\mu_{\mathrm{hnf}}}{(\rho C_p)_{\mathrm{hnf}}}\left(\frac{\partial u}{\partial y}\right)^2. \tag{4}$$

with conditions of:

$$u = U_w + L\frac{\partial u}{\partial y}, \quad v = 0, \quad N = -m\frac{\partial u}{\partial y}, \quad T = T_f = T_\infty + cx \text{ at } y$$
$$= 0 \ u \to U_\infty, \ N \to 0, \ T \to T_\infty \text{ as } y \to \infty \tag{5}$$

The velocities in directions of x and y are u and v, independently, T is the nanofluid temperature, and L is the slip length. In addition, N refers to the angular velocity in the xy-plane, k refers to vortex viscosity, $j = \frac{\nu_f}{b}$ is the density of micro inertial and $\varsigma = \left(\mu_f + \frac{\kappa}{2}\right)j$ is the spin gradient viscosity.[31] Additionally, m is a constant between [0,1]. When $m = 0$, that also signifies that $N = 0$; the microelements close to the surface cannot spin, which represents concentrated particle flows[32] or cited in Smith and Guram,[33] due to the concentrated microelements.

Table 1 Physical characteristics of the water−based Cu−Al$_2$O$_3$ (ref. 17)

Properties	Hybrid nanofluid
Dynamic viscosity	$\dfrac{\mu_{\text{hnf}}}{\mu_{\text{f}}} = (1 - \varphi_1)^{-2.5}(1 - \varphi_2)^{-2.5}$
Heat capacity	$(\rho C_{\text{p}})_{\text{hnf}} = \varphi_2(\rho C_{\text{p}})_{\text{s2}} + (1 - \varphi_2)[(1 - \varphi_1)(\rho C_{\text{p}})_{\text{f}} + \varphi_1(\rho C_{\text{p}})_{\text{s1}}]$
Thermal conductivity	$\dfrac{k_{\text{hnf}}}{k_{\text{bf}}} = \dfrac{k_{\text{s2}} + 2k_{\text{bf}} - 2\varphi_2(k_{\text{bf}} - k_{\text{s2}})}{k_{\text{s2}} + 2k_{\text{bf}} + \varphi_2(k_{\text{bf}} - k_{\text{s2}})}$ where $\dfrac{k_{\text{bf}}}{k_{\text{f}}} = \dfrac{k_{\text{s1}} + 2k_{\text{f}} - 2\varphi_1(k_{\text{f}} - k_{\text{s1}})}{k_{\text{s1}} + 2k_{\text{f}} + \varphi_1(k_{\text{f}} - k_{\text{s1}})}$
Electrical conductivity	$\dfrac{\sigma_{\text{hnf}}}{\sigma_{\text{bf}}} = \dfrac{\sigma_{\text{s2}} + 2\sigma_{\text{bf}} - 2\varphi_2(\sigma_{\text{bf}} - \sigma_{\text{s2}})}{\sigma_{\text{s2}} + 2\sigma_{\text{bf}} + \varphi_2(\sigma_{\text{bf}} - \sigma_{\text{s2}})}$ where $\dfrac{\sigma_{\text{bf}}}{\sigma_{\text{f}}} = \dfrac{\sigma_{\text{s1}} + 2\sigma_{\text{f}} - 2\varphi_1(\sigma_{\text{f}} - \sigma_{\text{s1}})}{\sigma_{\text{s1}} + 2\sigma_{\text{f}} + \varphi_1(\sigma_{\text{f}} - \sigma_{\text{s1}})}$
Density	$\rho_{\text{Hbnf}}/\rho_{\text{f}} = \phi_{\text{Cu}}(\rho_{\text{Cu}}/\rho_{\text{f}}) + \phi_{\text{Al}_2\text{O}_3}(\rho_{\text{Al}_2\text{O}_3}/\rho_{\text{f}}) + (1 - \phi_{\text{Cu}} - \phi_{\text{Al}_2\text{O}_3})$

Table 2 Thermophysical properties of the nanoparticles and base fluid[40]

	c_{p} (J kg^{-1} K^{-1})	P (kg m^{-3})	K (W mK^{-1})	σ (S m^{-1})
Water	4179	997.1	0.613	0.05
Cu	385	8933	400	5.96×10^7
Al$_2$O$_3$	765	3970	40	3.69×10^7

However, the stress tensor anti-symmetric portion dissipates when $n = 0.5$ (low microelement concentration).[31] Additionally, the situation $n = 1$ is used to describe a flow with turbulence.[34]

2.2. Thermophysical features of hybrid nanofluids

Table 1 displays the physical characteristics of hybrid nanofluids, with subscripts hnf, otherwise nf, f and s, indicating nanofluid, fluid, and nanoparticle, respectively. The first and second nanoparticles are denoted as s1 and s2, respectively, where φ_1 is the volume fraction of alumina (Al$_2$O$_3$), and φ_2 that of copper (Cu), while water is the base fluid.

Further, the thermophysical experimental data of the base fluid (water) and the hybrid nanoparticles (copper and silver) are given in Table 2.

2.3. Similarity transformation

To facilitate the analysis of the problem at hand, we hereby introduce the following set of similarity variables, which can be employed:

$$\psi = (\nu_{\text{f}}b)^{1/2}x f(\eta), \quad \eta = \left(\frac{b}{\nu_{\text{f}}}\right)^{1/2}, \quad N = bx\left(\frac{b}{\nu_{\text{f}}}\right)^{1/2} h(\eta), \quad \theta(\eta)$$

$$= \frac{T - T_\infty}{T_{\text{f}} - T_\infty} \tag{6}$$

By introducing the stream function $u = \dfrac{\partial \psi}{\partial y}$ and $v = -\dfrac{\partial \psi}{\partial x}$ which satisfy eqn (1), then eqn (1)–(4) and conditions (5) are written as follows:

$$\left[\frac{\mu_{\text{hnf}}/\mu_f}{\rho_{\text{hnf}}/\rho_f} + \frac{K}{\rho_{\text{hnf}}/\rho_f}\right]f''' + ff'' - f'^2 + \frac{K}{\rho_{\text{hnf}}/\rho_f}h'$$
$$+ \frac{\sigma_{\text{hnf}}/\sigma_f}{\rho_{\text{hnf}}/\rho_f}M(1 - f') = 0 \tag{7}$$

$$\left[\frac{\mu_{\text{hnf}}/\mu_f}{\rho_{\text{hnf}}/\rho_f} + \frac{K}{2(\rho_{\text{hnf}}/\rho_f)}\right]h'' + fh' - f'h - \frac{K}{\rho_{\text{hnf}}/\rho_f}(2h + f'') = 0 \tag{8}$$

$$\frac{1}{\text{Pr}}\frac{k_{\text{hnf}}/k_f}{(\rho C_{\text{p}})_{\text{hnf}}/(\rho C_{\text{p}})_f}\theta'' + f\theta' - f'\theta$$
$$+ Ec\left[\begin{array}{c}\dfrac{\sigma_{\text{hnf}}/\sigma_f}{(\rho C_{\text{p}})_{\text{hnf}}/(\rho C_{\text{p}})_f}M(1 - f')^2 \\ + \dfrac{\mu_{\text{hnf}}/\mu_f}{(\rho C_{\text{p}})_{\text{hnf}}/(\rho C_{\text{p}})_f}f''^2\end{array}\right] = 0 \tag{9}$$

$$f(0) = 0, f'(0) = \varepsilon + \lambda f''(0), h(0) = -mf''(0), \theta(0) = 1, f'(\eta) \to 1, h(\eta) \to 0, \theta(\eta) \to 0 \tag{10}$$

where $\lambda = L\left(\dfrac{b}{\nu_{\text{f}}}\right)^{1/2}$ is the slip parameter and $\varepsilon = \dfrac{a}{b}$ is the velocity ratio parameter such that $\varepsilon < 0$ is for shrinking conditions and $\varepsilon > 0$ for stretching conditions.

2.4. Skin friction coefficient and local Nusselt number

The skin friction coefficient C_{f} and the local Nusselt number Nu_x are written as

$$C_{\text{f}} = \frac{1}{\rho_{\text{f}}U_\infty^2}\left[(\mu_{\text{hnf}} + \kappa)\frac{\partial u}{\partial y} + \kappa N\right]_{y=0},$$
$$\text{Nu}_x = \frac{-x}{k_{\text{f}}(T_{\text{f}} - T_\infty)}\left[k_{\text{hnf}}\left(\frac{\partial T}{\partial y}\right)\right]_{y=0}, \tag{11}$$

After performing the transformations,

$$C_f(\mathrm{Re}_x)^{1/2} = \left[\frac{\mu_{hnf}}{\mu_f} + (1-m)K\right]f''(0), \ \mathrm{Nu}_x(\mathrm{Re}_x)^{-1/2}$$

$$= \frac{-k_{hnf}}{k_f}\theta'(0), \tag{12}$$

where $\mathrm{Re}_x = \dfrac{U_\infty x}{v_f}$ is the local Reynolds number.

2.5. Stability analysis

To further check the obtained solutions, an analysis of stability is performed. The results of this analysis support the interpretation that solely the first solution is stable whilst not the other one, which has been validated by several researchers.[35–37] In order to perturb eqn (2)–(4), the unsteady case is introduced, and hence we write as

$$\frac{\partial u}{\partial t} + u\frac{\partial u}{\partial x} + v\frac{\partial u}{\partial y} = U_\infty\frac{dU_\infty}{dx} + \frac{\mu_{hnf} + \kappa}{\rho_{hnf}}\frac{\partial^2 u}{\partial y^2} + \frac{\kappa}{\rho_{hnf}}\frac{\partial N}{\partial y}$$

$$+ \frac{\sigma_{hnf}B_0^2}{\rho_{hnf}}(U_\infty - u), \tag{13}$$

$$\frac{\partial N}{\partial t} + u\frac{\partial N}{\partial x} + v\frac{\partial N}{\partial y} = \frac{\varsigma}{\rho_{hnf}j}\frac{\partial^2 N}{\partial y^2} - \frac{\kappa}{\rho_{hnf}j}\left(2N + \frac{\partial u}{\partial y}\right), \tag{14}$$

$$\frac{\partial T}{\partial t} + u\frac{\partial T}{\partial x} + v\frac{\partial T}{\partial y} = \frac{k_{hnf}}{(\rho C_p)_{hnf}}\frac{\partial^2 T}{\partial r^2} + \frac{\sigma_{hnf}B_0^2}{(\rho C_p)_{hnf}}(U_\infty - u)^2$$

$$+ \frac{\mu_{hnf}}{(\rho C_p)_{hnf}}\left(\frac{\partial u}{\partial y}\right)^2. \tag{15}$$

The following new similarity transformation is proposed:

$$\psi = (v_f b)^{1/2}xf(\eta, \tau), \ \eta = \left(\frac{b}{v_f}\right)^{1/2},$$

$$N = bx\left(\frac{b}{v_f}\right)^{1/2}h(\eta, \tau), \ \theta(\eta, \tau) = \frac{T - T_\infty}{T_f - T_\infty} \ \tau = bt, \tag{16}$$

By applying eqn (16) to eqn (13)–(15), the subsequent expressions are obtained:

$$\left[\frac{\mu_{hnf}/\mu_f}{\rho_{hnf}/\rho_f} + \frac{K}{\rho_{hnf}/\rho_f}\right]\frac{\partial^3 f}{\partial\eta^3} + f\frac{\partial^2 f}{\partial\eta^2} - \left(\frac{\partial f}{\partial\eta}\right)^2 + 1 + \frac{K}{\rho_{hnf}/\rho_f}\frac{\partial h}{\partial\eta}$$

$$+ \frac{\sigma_{hnf}/\sigma_f}{\rho_{hnf}/\rho_f}M\left(1 - \frac{\partial f}{\partial\eta}\right) - \frac{\partial^2 f}{\partial\eta\partial\tau} = 0 \tag{17}$$

$$\left[\frac{\mu_{hnf}/\mu_f}{\rho_{hnf}/\rho_f} + \frac{K}{2(\rho_{hnf}/\rho_f)}\right]\frac{\partial^2 h}{\partial\eta^2} + f\frac{\partial h}{\partial\eta} - h\frac{\partial f}{\partial\eta} - \frac{K}{\rho_{hnf}/\rho_f}\left(2h + \frac{\partial^2 f}{\partial\eta^2}\right)$$

$$- \frac{\partial h}{\partial\tau} = 0 \tag{18}$$

$$\frac{1}{\mathrm{Pr}}\frac{k_{hnf}/k_f}{(\rho C_p)_{hnf}/(\rho C_p)_f}\frac{\partial^2\theta}{\partial\eta^2} + f\frac{\partial\theta}{\partial\eta} - \frac{\partial f}{\partial\eta}\theta$$

$$+ Ec\left[\frac{\sigma_{hnf}/\sigma_f}{(\rho C_p)_{hnf}/(\rho C_p)_f}M\left(1 - \frac{\partial f}{\partial\eta}\right)^2\right.$$

$$+ \left.\frac{\mu_{hnf}/\mu_f}{(\rho C_p)_{hnf}/(\rho C_p)_f}\left(\frac{\partial^2 f}{\partial\eta^2}\right)^2\right] - \frac{\partial\theta}{\partial\tau}$$

$$= 0 \tag{19}$$

with conditions of:

$$f(0, \tau) = 0, \ \frac{\partial f}{\partial\eta}(0, \tau) = \varepsilon + \lambda\frac{\partial^2 f}{\partial\eta^2}(0, \tau), \ h(0, \tau)$$

$$= -m\frac{\partial^2 f}{\partial\eta^2}(0, \tau), \ \theta(0, \tau)$$

$$= 1, \ \frac{\partial f}{\partial\eta}(\eta, \tau) \to 1, \ h(\eta, \tau) \to 0, \ \theta(\eta, \tau) \to 0 \tag{20}$$

Table 3 Comparison value of $f''(0)$ for different ε when $\varphi_1 = \varphi_2 = K = M = n = 0^a$

ε	Zainal et al.[41]	Anuar et al.[30]	Present
−0.25	1.40221	1.40221	1.40221
−0.5	1.495670	1.495670	1.495670
−0.75	1.489298	1.489298	1.489298
−1	1.328817	1.328817	1.328817
	[0]	[0]	[0]
−1.1	1.186680	1.186680	1.186680
	[0.049229]	[0.049229]	[0.049229]
−1.15	1.082231	1.082231	1.082231
	[0.116702]	[0.116702]	[0.116702]
−1.2	0.932473	0.932473	0.932473
	[0.233650]	[0.233650]	[0.233650]
−1.246	0.609826	0.609826	0.609826
	[0.529035]	[0.529035]	[0.529035]
−1.2465	-	0.584282	0.584282
	-	[0.554296]	[0.554296]

^{a} [ ] Second solution.

Table 4 Values of $C_f(\mathrm{Re}_x)^{1/2}$ and $\mathrm{Nu}_x(\mathrm{Re}_x)^{-1/2}$ for various ε for the first solution

φ_2	ε	$C_f(\mathrm{Re}_x)^{1/2}$	$\mathrm{Nu}_x(\mathrm{Re}_x)^{-1/2}$
0	2	−1.77728	3.28277
	1	0	3.16126
	0	1.37770	1.14263
	−0.5	1.82975	−0.79907
	−1	1.99028	−4.06281
0.01	2	−1.84526	3.28115
	1	0	3.20568
	0	1.54532	1.14809
	−0.5	1.97168	−0.82816
	−1	2.04811	−4.07996
0.02	2	−1.91148	3.28011
	1	0	3.24999
	0	1.60478	1.15215
	−0.5	2.04992	−0.86128
	−1	2.13381	−4.11297
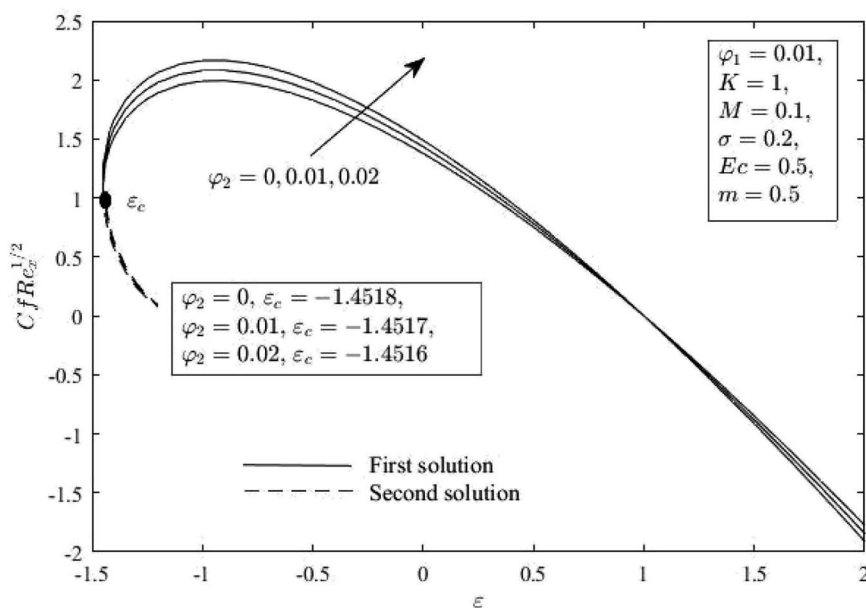
Fig. 2 $C_f(\mathrm{Re}_x)^{1/2}$ for φ_2 and ε.
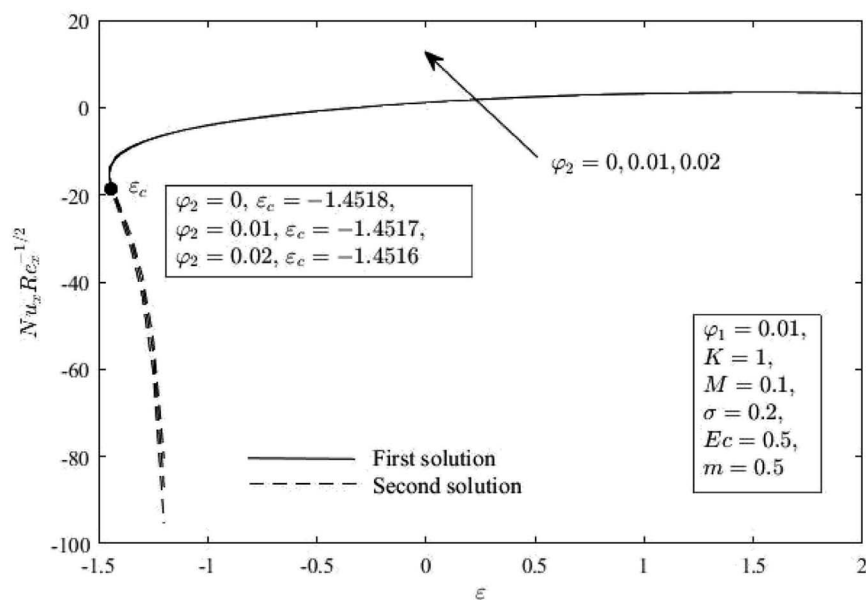
Fig. 3 $\mathrm{Nu}_x(\mathrm{Re}_x)^{-1/2}$ for φ_2 and ε.

Subsequently, to assess the stability, the subsequent equations are employed:[38]

$$f(\eta,\tau) = f_0(\eta) + \mathrm{e}^{-\gamma\tau}F(\eta,\tau),\ h(\eta,\tau) = h_0(\eta) + \mathrm{e}^{-\gamma\tau}H(\eta,\tau),\ \theta(\eta,\tau) = \theta_0(\eta) + \mathrm{e}^{-\gamma\tau}G(\eta,\tau) \quad (21)$$

where $F(\eta)$, $H(\eta)$ and $G(\eta)$ are low relative to $f_0(\eta)$, $h_0(\eta)$, $\theta_0(\eta)$, correspondingly, and γ is the eigenvalue. Applying eqn (21) to

(17)–(19), letting $\tau \to 0$, $F(\eta) = F_0(\eta)$, $H(\eta) = H_0(\eta)$ and $G(\eta) = G_0(\eta)$, one should get:

$$\left[\frac{\mu_{\mathrm{hnf}}/\mu_f}{\rho_{\mathrm{hnf}}/\rho_f} + \frac{K}{\rho_{\mathrm{hnf}}/\rho_f} \right] F'''_0 + f_0 F''_0 + F_0 f''_0 + \frac{K}{\rho_{\mathrm{hnf}}/\rho_f} H'_0$$

$$- \left[2f'_0 - \frac{\sigma_{\mathrm{hnf}}/\sigma_f}{\rho_{\mathrm{hnf}}/\rho_f} M - \gamma \right] f'_0 = 0 \quad (22)$$
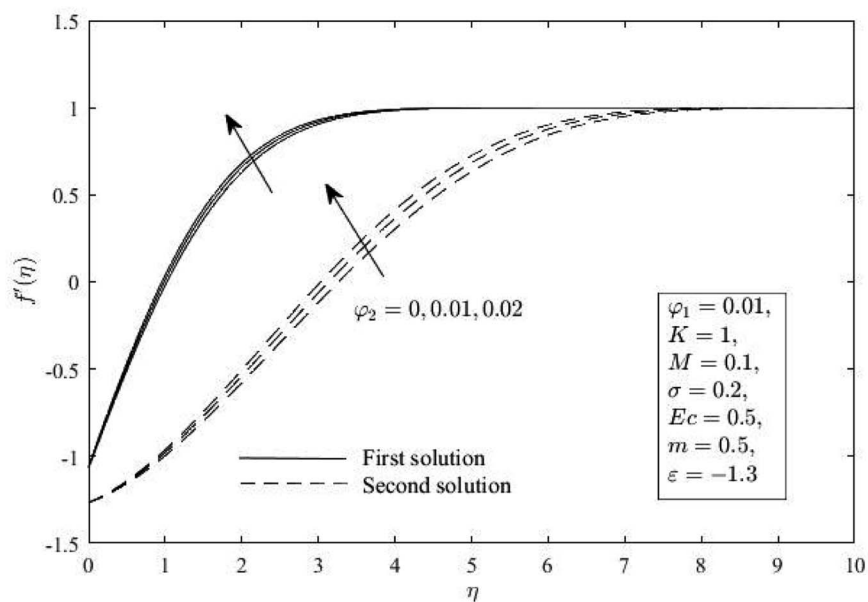
Fig. 4 $f'(\eta)$ for various φ_2.
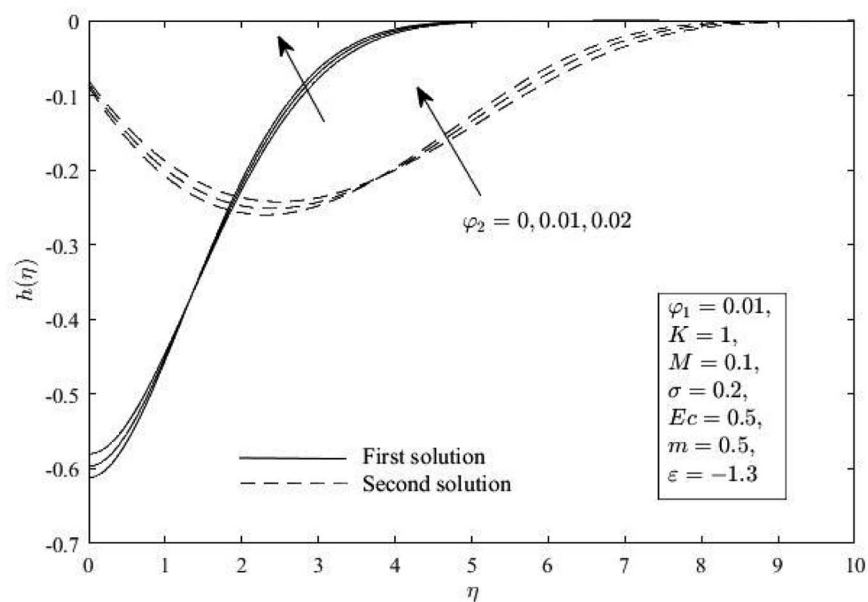
Fig. 5 $h(\eta)$ for various φ_2.

$$\left[\frac{\mu_{\mathrm{hnf}}/\mu_f}{\rho_{\mathrm{hnf}}/\rho_{\mathrm{f}}}+\frac{K}{2(\rho_{\mathrm{hnf}}/\rho_{\mathrm{f}})}\right]H''_0+f_0H'_0-F_0h'_0-h_0F'_0-H_0f'_0$$

$$-\frac{K}{\rho_{\mathrm{hnf}}/\rho_{\mathrm{f}}}(2H_0+f''_0)+\gamma H_0=0 \qquad (23)$$

$$\frac{k_{\mathrm{hnf}}/k_{\mathrm{f}}}{\Pr(\rho C_{\mathrm{p}})_{\mathrm{hnf}}/(\rho C_{\mathrm{p}})_{\mathrm{f}}}G''_0+F_0\theta'_0+f_0G'_0-f'_0G_0-F'_0\theta_0+\gamma G_0$$

$$+Ec\left[2\frac{\sigma_{\mathrm{hnf}}/\sigma_{\mathrm{f}}}{(\rho C_{\mathrm{p}})_{\mathrm{hnf}}/(\rho C_{\mathrm{p}})_{\mathrm{f}}}M(f'_0F'_0-F'_0)\right.$$

$$\left.+2\frac{\mu_{\mathrm{hnf}}/\mu_{\mathrm{f}}}{(\rho C_{\mathrm{p}})_{\mathrm{hnf}}/(\rho C_{\mathrm{p}})_{\mathrm{f}}}f''_0F''_0\right]$$

$$=0 \qquad (24)$$
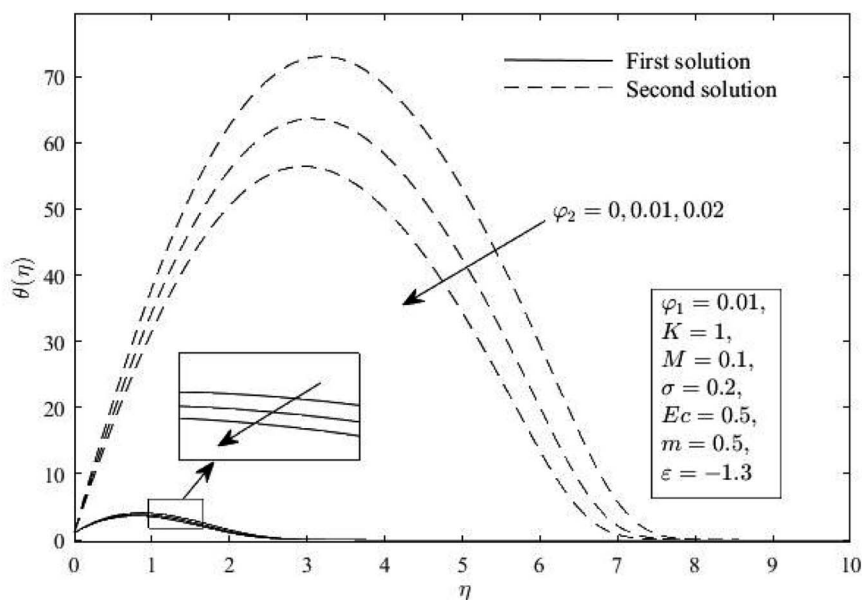
Fig. 6 $\theta(\eta)$ for various φ_2.
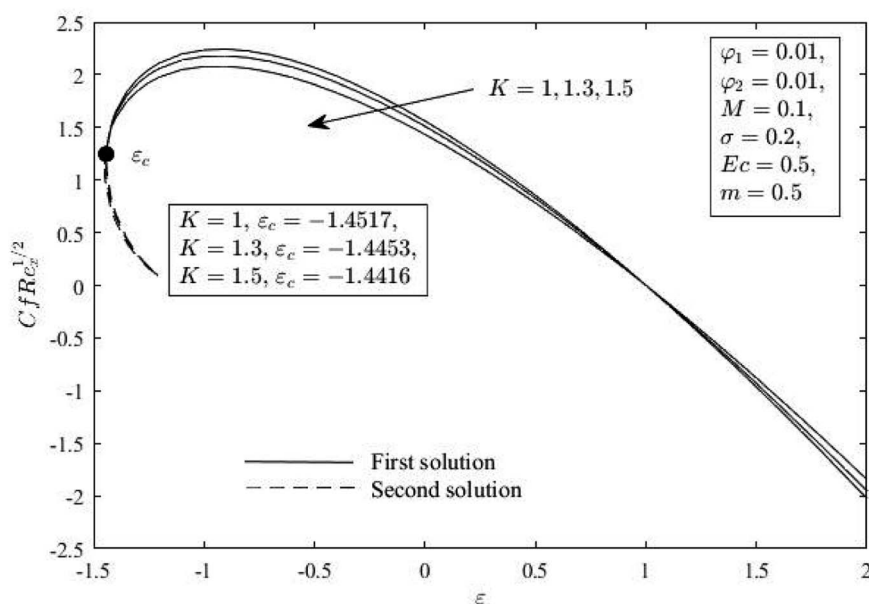
Fig. 7 $C_f(Re_x)^{1/2}$ for K and ε.

$$F_0(0) = G_0(0) = 0, \quad F'_0(0) = \lambda F''_0(0), \quad H_0(0)$$
$$= -mF''_0(0), \quad F'_0(\infty), \quad H_0(\infty), \quad G_0(\infty) \to 0. \quad (25)$$

It was necessary to relax a boundary condition with reference to Harris *et al.*[39] Therefore, we made modifications by setting $F'_0(\eta \to \infty) \to 0$, and introducing a new condition of $F''_0(\eta = 0) = 1$.

3. Results and discussion

Eqn (7)–(9) with eqn (10) are solved with the facilitation of bvp4c (Matlab). It is crucial to remember that in regards to the synthesis of the intended hybrid nanofluid, which is Cu–Al_2O_3/water, Al_2O_3 is first disseminated in water, and then Cu is added to it. The volume fraction of Al_2O_3 is constantly set up at 1 percent, while the fraction of Cu varies from 0 to 2 percent.
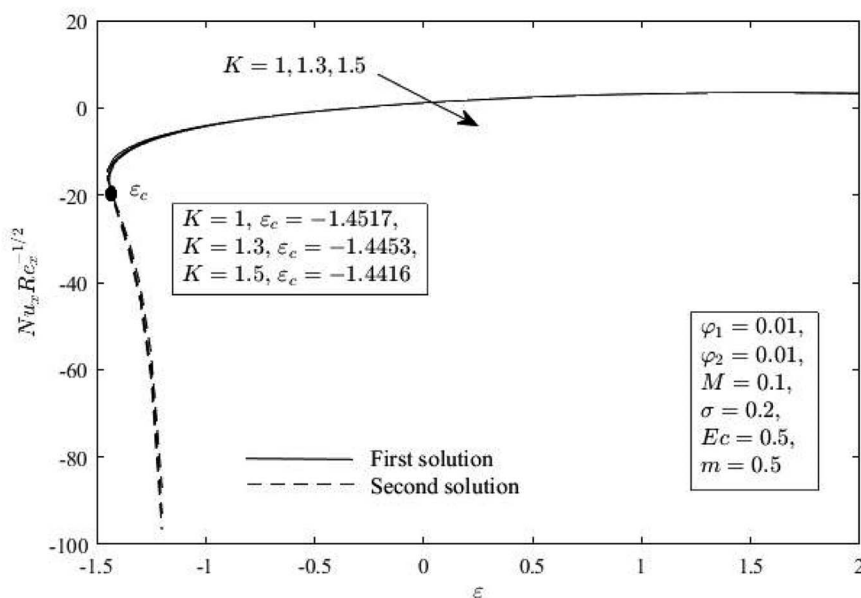
Fig. 8 $Nu_x(Re_x)^{-1/2}$ for K and ε.

The outcomes of the comparison and variation of $f''(0)$ with earlier research are exemplified in Table 3. The strong agreement between the results provides assurance that the numerical outcomes obtained are valid. In addition, Table 4 signifies the values of $C_f(Re_x)^{1/2}$ and $Nu_x(Re_x)^{-1/2}$ for various values of the ε and nanoparticle volume fraction for the branch of first solution. It shows that for each fixed value of the nanoparticle as ε increases, as a result, the $C_f(Re_x)^{1/2}$ increases, but $Nu_x(Re_x)^{-1/2}$ acts in an opposite manner.

Fig. 2 and 3 reveal how the Cu nanoparticle volume fraction φ_2 affects the distribution of $C_f(Re_x)^{1/2}$ and $Nu_x(Re_x)^{-1/2}$ as indicated in eqn (12) when compared to stretch or shrink parameter ε. When $\varepsilon_c < \varepsilon \leq -1$, dual solutions are present, while one solution is present when $\varepsilon > -1$, and there is no solution when $\varepsilon < \varepsilon_c < 0$, such that ε_c denotes the critical value of ε. It is obvious that the issue becomes micropolar nanofluid for $\varphi_2 = 0$. These figures show that an increase in φ_2 improves the $C_f(Re_x)^{1/2}$ and $Nu_x(Re_x)^{-1/2}$ for all ranges of ε in the first solution, but only slightly so in the second. This result demonstrates that
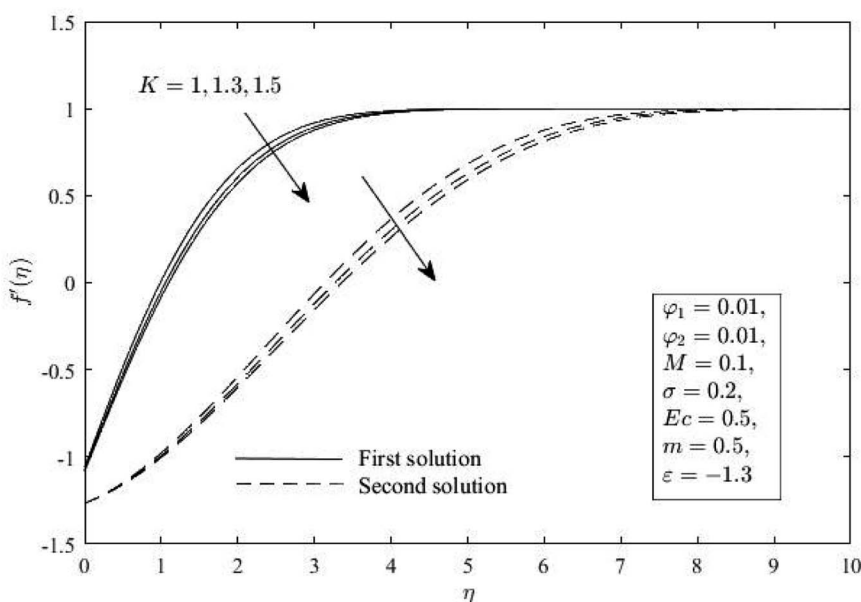

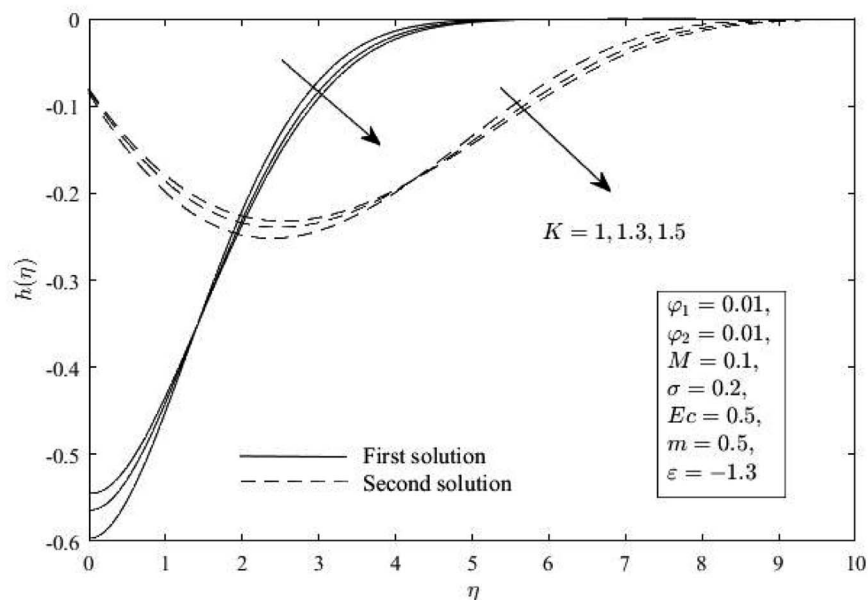Fig. 9 $f'(\eta)$ for various K.

Fig. 10 $h(\eta)$ for various K.

increasing φ_2 can increase the effectiveness of heat transmission. This suggests that hybrid nanofluid has superior thermal performance compared to nanofluid. Additionally, the skin friction coefficient and heat transfer rate accelerate the flow separation with higher impacts of the solid nanoparticle volume fraction (φ_2).

The impacts of φ_2 on the distribution of $f'(\eta)$, $h(\eta)$ and $\theta(\eta)$ for shrinking sheets ($\varepsilon = -1.3$) are demonstrated in Fig. 4–6. The outcomes show that both solutions, increasing φ_2 deflates the

boundary layer thickness of momentum, microrotation, and thermal. Physically, the thermal conductivity of the fluid (TCN) boosted up with higher φ_2, and as a response, the heat transfer rate increases for the stable outcomes. Additionally, all published profiles asymptotically satisfied the conditions (10) which ultimately confirmed the results shown in Fig. 2 and 3.

Fig. 7–11 show how the K affects $C_f(\mathrm{Re}_x)^{1/2}$ and $\mathrm{Nu}_x(\mathrm{Re}_x)^{-1/2}$, $f'(\eta)$, $h(\eta)$ and $\theta(\eta)$. Comparing the presence of K ($K = 1,2$) to the exclusion of K ($K = 0$), or the lack of vortex viscosity, it is clear
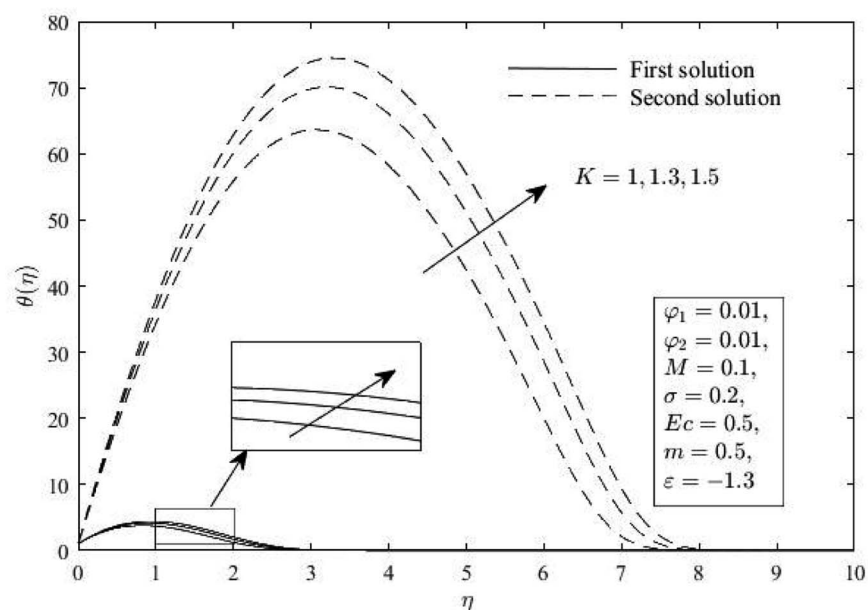

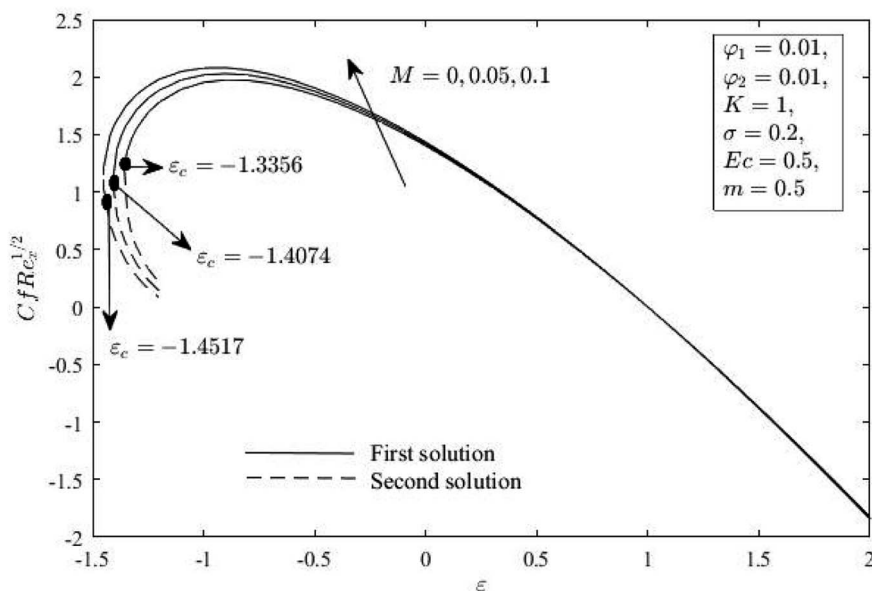**Fig. 11** $\theta(\eta)$ for various K.
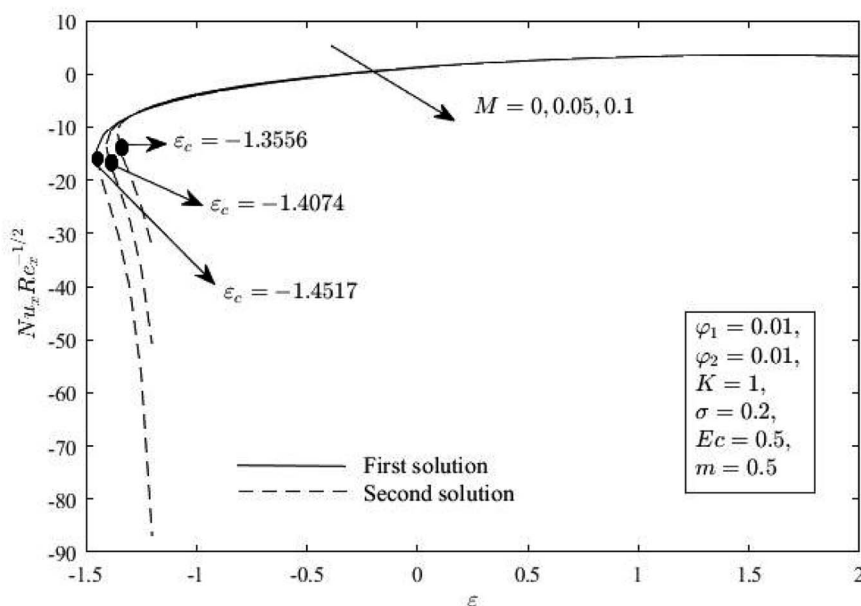
Fig. 12 $C_f(\mathrm{Re}_x)^{1/2}$ for M and ε.

Fig. 13 $\mathrm{Nu}_x(\mathrm{Re}_x)^{-1/2}$ for M and ε.

that the presence of K generates the $C_f(\mathrm{Re}_x)^{1/2}$. Different outcomes, however, are shown for $\mathrm{Nu}_x(\mathrm{Re}_x)^{-1/2}$. The absence of the micropolar fluid ($K = 0$) results in an improvement over the presence of K ($K = 1,2$). This phenomenon shows that the increment of K causes a fluid flow to become more viscous in a vortex, which increases $C_f(\mathrm{Re}_x)^{1/2}$ near the wall and slows $\mathrm{Nu}_x(\mathrm{Re}_x)^{-1/2}$. Additionally, both solutions' momentum and microrotation boundary layers became thicker because of the

increment of K. For the thermal boundary layer thickness, the results are the opposite.

Next, Fig. 12 and 13 show the effect of M on $C_f(\mathrm{Re}_x)^{1/2}$ and $\mathrm{Nu}_x(\mathrm{Re}_x)^{-1/2}$. These figures show that as M increases, $C_f(\mathrm{Re}_x)^{1/2}$ increases, but $\mathrm{Nu}_x(\mathrm{Re}_x)^{-1/2}$ is reduced. This is because the magnetic field induces a resistance force on the flow, consequently retarding the momentum of the fluid and improving $C_f(\mathrm{Re}_x)^{1/2}$. On the other side, $f'(\eta)$, $h(\eta)$ and $\theta(\eta)$ for various M are portrayed in Fig. 14–16. When M increases, the first solution's
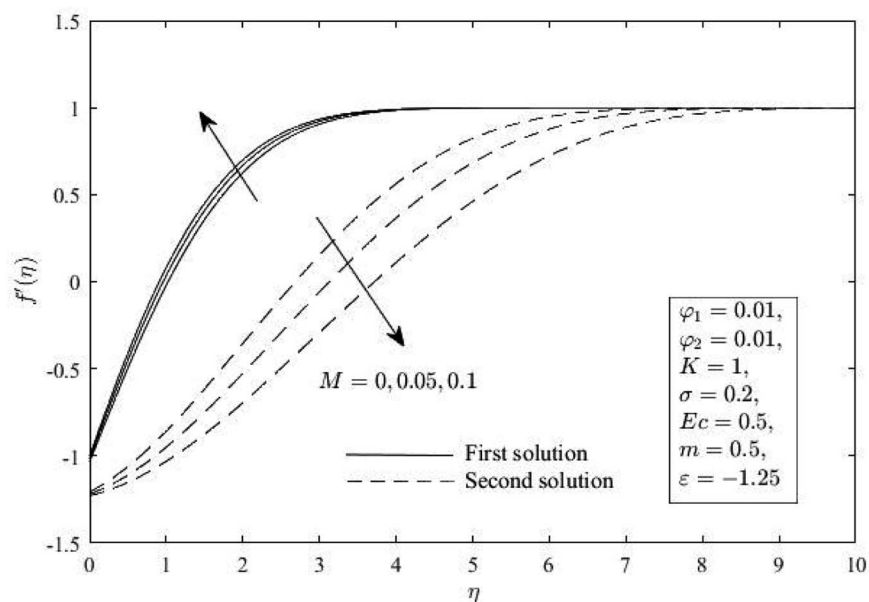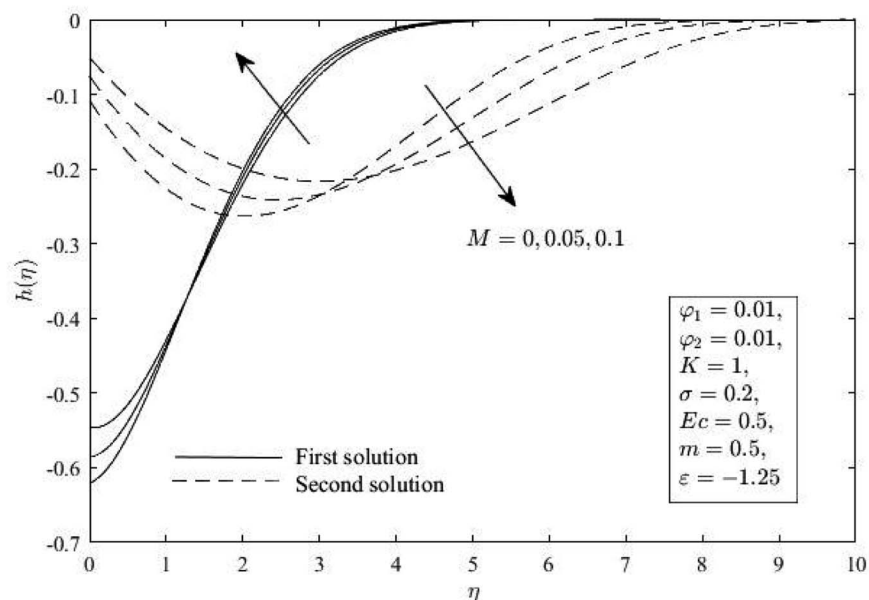
Fig. 14 $f'(\eta)$ for various M.

Fig. 15 $h(\eta)$ for various M.

diminished momentum, microrotation, and thermal boundary layer thickness are noted, whereas the second solution's opposite observation is noted. This is because the Lorentzian magneto-hydrodynamic component in the momentum equation is a drag force which acts in the negative axial direction transverse to the line of application which is in the positive transverse direction. With greater M, the magnetic field strength also increases, which enhances the momentum and thermal boundary layer thickness.

Fig. 17 illustrates the minimum eigenvalues γ plotted against different values of ε. The graph unravels that the first solution displays $\gamma > 0$, whilst the second solution displays $\gamma < 0$. As $\varepsilon \to \varepsilon_c$, Fig. 8 shows that γ approaches zero for both similarity solutions, which confirms that γ equals zero when ε equals ε_c. Hence, out of the available solutions, only the first one remains stable.
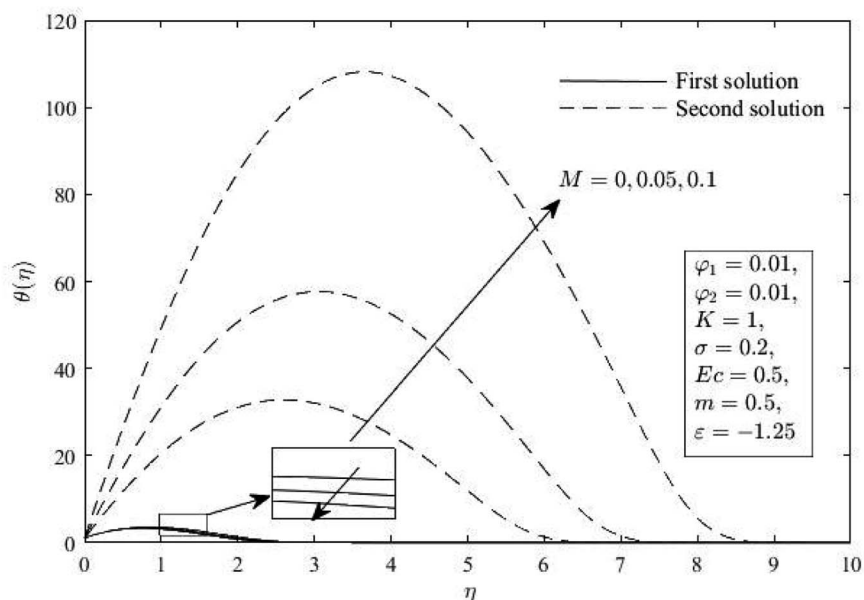
Fig. 16 $\theta(\eta)$ for various M.

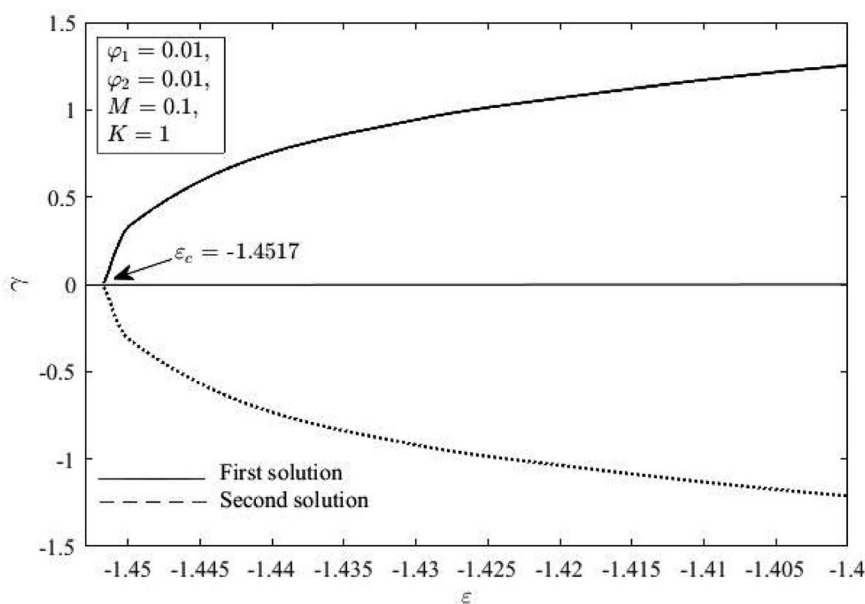**Fig. 17** Smallest eigenvalue γ against ε for $K = 1$, $\varphi_1 = \varphi_2 = 0.1$ and $M = 0.1$.

4. Conclusion

The MHD stagnation point flow of micropolar hybrid nanofluid with viscous dissipation *via* stretching/shrinking sheets was theoretically analyzed in this research. The problem at hand was successfully resolved with the aid of the Matlab bvp4c solver. The main takeaways are:

•Dual solutions are only available when $\varepsilon < 0$; however, only the first solution is stable.

•The increasing volume fraction φ_2 in the micropolar nanofluid results in an enhancement in both $C_f(\mathrm{Re}_x)^{1/2}$ and $\mathrm{Nu}_x(\mathrm{Re}_x)^{-1/2}$.

•The enlargement of material parameter K and MHD parameter M causes $C_f(\mathrm{Re}_x)^{1/2}$ to be improved and the opposite for the $\mathrm{Nu}_x(\mathrm{Re}_x)^{-1/2}$.

•The domains of the similarity solutions decrease with an increase in φ_2 and K, which therefore fastens the boundary layer separation. However, an increase in the value of M delays the boundary layer separation.

The findings of this study, limited to the chosen setup parameters, underscore the importance of considering that further improvements are needed to validate these conclusions in broader contexts. It is crucial to acknowledge that the current study should be extended to encompass various types of

nanoparticles and base fluids, with a particular emphasis on enhancing the model for ternary hybrid nanofluids.

Data availability

The data will be available on request to the corresponding author.

Conflicts of interest

It is declared that we have no conflict of interest.

Acknowledgements

References

1 K. Hiemenz, Die Grenzchicht an einem in den gleichformingen Flussigkeitsstrom eingetauchten geraden Kreiszylinder, *Dinglers Polytech. J.*, 1911, **326**, 391–393.

2 A. C. Eringen, Theory of micropolar fluids, *J. Math. Mech.*, 1966, 1–18.

3 S. K. Soid, A. Ishak and I. Pop, MHD stagnation-point flow over a stretching/shrinking sheet in a micropolar fluid with a slip boundary, *Sains Malays.*, 2018, **47**(11), 2907–2916.

4 N. S. Khashi'ie, N. Safwa, N. Md Arifin, R. Nazar, E. H. Hafidzuddin, N. Wahi and I. Pop, Mixed convective flow and heat transfer of a dual stratified micropolar fluid induced by a permeable stretching/shrinking sheet, *Entropy*, 2019, **21**(12), 1162.

5 S. R. Mishra, I. Khan, Q. M. Al-Mdallal and T. Asifa, Free convective micropolar fluid flow and heat transfer over a shrinking sheet with heat source, *Case Stud. Therm. Eng.*, 2018, **11**, 113–119.

6 L. A. Lund, Z. Omar, I. Khan, B. Dumitru and K. S. Nisar, Triple solutions and stability analysis of micropolar fluid flow on an exponentially shrinking surface, *Crystals*, 2020, **10**(4), 283.

7 R. I. Yahaya, N. Md Arifin, S. S. P. Mohamed Isa and M. M. Rashidi, Magnetohydrodynamics boundary layer flow of micropolar fluid over an exponentially shrinking sheet with thermal radiation: Triple solutions and stability analysis, *Math. Methods Appl. Sci.*, 2021, **44**(13), 10578–10608.

8 S. U. S. Choi, and J. A. Eastman, *Enhancing Thermal Conductivity of Fluids with Nanoparticles*, No. ANL/MSD/CP-84938; CONF-951135-29, Argonne National Lab.ANL, Argonne, IL United States, 1995.

9 N. H. Abd Rahman, N. Hathirah, N. Bachok and H. Rosali, MHD Stagnation-point Flow over a Stretching/Shrinking Sheet in Nanofluids, *J. Adv. Res. Fluid Mech. Therm. Sci.*, 2019.

10 N. H. A. Norzaway, N. Bachok and F. M. Ali, Stagnation Point Flow over a Stretching/shrinking Sheet in a Carbon Nanotubes with Suction/Injection Effects, *CFD Lett.*, 2020, **12**(2), 106–114.

11 N. S. Wahid, N. Md Arifin, I. Pop, N. Bachok and M. E. H. Hafidzuddin, MHD stagnation-point flow of nanofluid due to a shrinking sheet with melting, viscous dissipation and Joule heating effects, *Alexandria Eng. J.*, 2022, **61**(12), 12661–12672.

12 S. T. Hussain, S. Nadeem and R. Ul Haq., Model-based analysis of micropolar nanofluid flow over a stretching surface, *Eur. Phys. J. Plus*, 2014, **129**, 1–10.

13 H. R. Patel, A. S. Mittal and R. R. Darji, MHD flow of micropolar nanofluid over a stretching/shrinking sheet considering radiation, *Int. Commun. Heat Mass Transfer*, 2019, **108**, 104322.

14 L. A. Lund, Z. Omar, U. Khan, I. Khan, B. Dumitru and K. S. Nisar, Stability analysis and dual solutions of micropolar nanofluid over the inclined stretching/ shrinking surface with convective boundary condition, *Symmetry*, 2020, **12**(1), 74.

15 M. Atif Shahzada, M. Abbas, U. Rashid and H. Emadifar, Stagnation point flow of EMHD micropolar nanofluid with mixed convection and slip boundary, *Complexity*, 2021, **2021**, 1–13.

16 D. Madhesh and S. Kalaiselvam, Experimental analysis of hybrid nanofluid as a coolant, *Procedia Eng.*, 2014, **97**, 1667–1675.

17 S. U. Devi and S. P. A. Devi, Heat transfer enhancement of cu$-$al$_2$o$_3$/water hybrid nanofluid flow over a stretching sheet, *J. Niger. Soc. Math.*, 2017, **36**(2), 419–433.

18 R. I. Yahaya, N. M. Arifin, R. Nazar and I. Pop, Flow and heat transfer past a permeable stretching/shrinking sheet in Cu$-$Al2O3/water hybrid nanofluid, *Int. J. Numer. Methods Heat Fluid Flow*, 2020, **30**(3), 1197–1222.

19 N. S. Anuar, N. Bachok and I. Pop, Influence of buoyancy force on Ag-MgO/water hybrid nanofluid flow in an inclined permeable stretching/shrinking sheet, *Int. Commun. Heat Mass Transfer*, 2021, **123**, 105236.

20 N. S. Wahid, N. Md Arifin, N. S. Khashi'ie and I. Pop, Mixed convection MHD hybrid nanofluid over a shrinking permeable inclined plate with thermal radiation effect, *Alexandria Eng. J.*, 2023, **66**, 769–783.

21 M. Sarfraz, M. Khan and Y. Muhammad, Dynamic of water conveying iron oxide and graphene nanoparticles subject to stretching/spiraling surface: An asymptotic approach, *Ain Shams Eng. J.*, 2023, **14**, 102021.

22 M. Yasir, M. Sarfraz, M. Khan, A. K. Alzahrani and M. Z. Ullah, Estimation of dual branch solutions for Homann flow of hybrid nanofluid towards biaxial shrinking surface, *J. Pet. Sci. Eng.*, 2022, **218**, 110990.

23 M. Sarfraz and M. Khan, Thermodynamic irreversibility analysis of water conveying argentum and titania nanoparticles subject to inclined stretching surface, *Phys. Scr.*, 2023, **98**, 025205.

24 M. Sarfraz, Y. Muhammad and M. Khan, Multiple solutions for non-linear radiative mixed convective hybrid nanofluid flow over an exponentially shrinking surface, *Nature*, 2023, **13**, 3443.

25 M. Subhani and S. Nadeem, Numerical analysis of micropolar hybrid nanofluid, *Appl. Nanosci.*, 2019, **9**(4), 447–459.

26 F. Kamal, K. Zaimi, A. Ishak and I. Pop, Stability analysis of MHD stagnation-point flow towards a permeable stretching/ shrinking sheet in a nanofluid with chemical reactions effect, *Sains Malays.*, 2019, **48**(1), 243–250.

27 A. Yasmin, K. Ali and M. Ashraf, Study of heat and mass transfer in MHD flow of micropolar fluid over a curved stretching sheet, *Sci. Rep.*, 2020, **10**(1), 4581.

28 A. Ishak, Y. Y. Lok and I. Pop, Stagnation-point flow over a shrinking sheet in a micropolar fluid, *Chem. Eng. Commun.*, 2010, **197**(11), 1417–1427.

29 L. A. Lund, Z. Omar, I. Khan, J. Raza, M. El-Sayed Sherif and H. S. Asiful, "Magnetohydrodynamic (MHD) flow of micropolar fluid with effects of viscous dissipation and joule heating over an exponential shrinking sheet: triple solutions and stability analysis, *Symmetry*, 2020, **12**(1), 142.

30 N. S. Anuar and N. Bachok, Double solutions and stability analysis of micropolar hybrid nanofluid with thermal radiation impact on unsteady stagnation point flow, *Mathematics*, 2021, **9**(3), 276.

31 G. Ahmadi, Self-similar solution of imcompressible micropolar boundary layer flow over a semi-infinite plate, *Int. J. Eng. Sci.*, 1976, **14**(7), 639–646.

32 S. Ko Jena and M. N. Mathur, Similarity solutions for laminar free convection flow of a thermomicropolar fluid past a non-isothermal vertical flat plate, *Int. J. Eng. Sci.*, 1981, **19**(11), 1431–1439.

33 G. S. Guram and A. C. Smith, Stagnation flows of micropolar fluids with strong and weak interactions, *Comput. Math. Appl.*, 1980, **6**(2), 213–233.

34 J. Peddieson Jr, An application of the micropolar fluid model to the calculation of a turbulent shear flow, *Int. J. Eng. Sci.*, 1972, **10**(1), 23–32.

35 N. S. Anuar, N. Bachok, N. M. Arifin and H. Rosali, MHD flow past a nonlinear stretching/shrinking sheet in carbon nanotubes: Stability analysis, *Chin. J. Phys.*, 2020, **65**, 436–446.

36 N. S. Anuar, N. Bachok, M. Turkyilmazoglu, N. M. Arifin and H. Rosali, Analytical and stability analysis of MHD flow past a nonlinearly deforming vertical surface in Carbon Nanotubes, *Alexandria Eng. J.*, 2020, **59**(1), 497–507.

37 A. Banerjee, K. Bhattacharyya, S. K. Mahato and A. J. Chamkha, Influence of various shapes of nanoparticles on unsteady stagnation-point flow of Cu-H2O nanofluid on a flat surface in a porous medium: A stability analysis, *Chin. Phys. B*, 2022, **31**(4), 044701.

38 P. D. Weidman, D. G. Kubitschek and A. M. J. Davis, The effect of transpiration on self-similar boundary layer flow over moving surfaces, *Int. J. Eng. Sci.*, 2006, **44**(11–12), 730–737.

39 S. D. Harris, D. B. Ingham and I. Pop, Mixed convection boundary-layer flow near the stagnation point on a vertical surface in a porous medium: Brinkman model with slip, *Transp. Porous Media*, 2009, **77**, 267–285.

40 H. F. Oztop and E. Abu-Nada, Numerical study of natural convection in partially heated rectangular enclosures filled with nanofluids, *Int. J. Heat Fluid Flow*, 2008, **29**(5), 1326–1336.

41 N. A. Zainal, R. Nazar, K. Naganthran and I. Pop, Unsteady stagnation point flow of hybrid nanofluid past a convectively heated stretching/shrinking sheet with velocity slip, *Mathematics*, 2020, **8**(10), 1649.